The Regulation of Photosynthetic Structure and Function during Nitrogen Deprivation in *Chlamydomonas reinhardtii*[1][OPEN]

Matthew T. Juergens, Rahul R. Deshpande, Ben F. Lucker, Jeong-Jin Park, Hongxia Wang, Mahmoud Gargouri, F. Omar Holguin, Bradley Disbrow, Tanner Schaub, Jeremy N. Skepper, David M. Kramer, David R. Gang, Leslie M. Hicks, and Yair Shachar-Hill*

Department of Plant Biology (M.T.J., R.R.D., B.D., Y.S.-H.) and Plant Research Laboratory (M.T.J., B.F.L., D.M.K.), Michigan State University, East Lansing, Michigan 48824; Institute of Biological Chemistry, Washington State University, Pullman, Washington 99164 (J.-J.P., M.G., D.R.G.); Donald Danforth Plant Science Center, St. Louis, Missouri 63132 (H.W., L.M.H.); National Center of Biomedical Analysis, Beijing 100850, China (H.W.); College of Agricultural, Consumer, and Environmental Sciences, New Mexico State University, Las Cruces, New Mexico 88003 (F.O.H., T.S.); Department of Physiology, Cambridge Advanced Imaging Centre, Cambridge CB2 3DY, United Kingdom (J.N.S.); and Department of Chemistry, University of North Carolina, Chapel Hill, North Carolina 27599 (L.M.H.)

The accumulation of carbon storage compounds by many unicellular algae after nutrient deprivation occurs despite declines in their photosynthetic apparatus. To understand the regulation and roles of photosynthesis during this potentially bioenergetically valuable process, we analyzed photosynthetic structure and function after nitrogen deprivation in the model alga *Chlamydomonas reinhardtii*. Transcriptomic, proteomic, metabolite, and lipid profiling and microscopic time course data were combined with multiple measures of photosynthetic function. Levels of transcripts and proteins of photosystems I and II and most antenna genes fell with differing trajectories; thylakoid membrane lipid levels decreased, while their proportions remained similar and thylakoid membrane organization appeared to be preserved. Cellular chlorophyll (Chl) content decreased more than 2-fold within 24 h, and we conclude from transcript protein and ^{13}C labeling rates that Chl synthesis was down-regulated both pre- and posttranslationally and that Chl levels fell because of a rapid cessation in synthesis and dilution by cellular growth rather than because of degradation. Photosynthetically driven oxygen production and the efficiency of photosystem II as well as $P700^+$ reduction and electrochromic shift kinetics all decreased over the time course, without evidence of substantial energy overflow. The results also indicate that linear electron flow fell approximately 15% more than cyclic flow over the first 24 h. Comparing Calvin-Benson cycle transcript and enzyme levels with changes in photosynthetic $^{13}CO_2$ incorporation rates also pointed to a coordinated multilevel down-regulation of photosynthetic fluxes during starch synthesis before the induction of high triacylglycerol accumulation rates.

Our current dependence on fossil fuels is unsustainable, motivating the development of bioenergy resources. Among these, microalgal oil and biomass production has shown promise (Chisti, 2007; Ohlrogge et al., 2009; Williams and Laurens, 2010; Atabani et al., 2012) because of the photoautotrophic growth of algae and their ability to reach high cell densities and accumulate high dry weight percentages of triacylglycerol (TAG) and their potential for much higher productivity per hectare than terrestrial biofuel crops (Hu et al., 2008; Wijffels and Barbosa, 2010). The unicellular green alga *Chlamydomonas reinhardtii* is among the most widely studied models of photosynthesis (Rochaix, 2002) and other cellular processes, including lipid accumulation by algae under stress (Merchant et al., 2012). Its advantages for studying photosynthetic mechanisms and regulation include the ability to grow both photo- and heterotrophically so that photosynthetic down-regulation and photosynthetically impaired mutants can be isolated (Dent et al., 2001) and a fully sequenced genome, collections of mutants, and the ease with which its growth, physiology, and photosynthetic rates can be measured.

In a range of microalgae, nitrogen (N) deprivation induces high accumulation of starch and TAG (Martin and Goodenough, 1975; Shifrin and Chisholm, 1981; Granum et al., 2002; Hu et al., 2008; Liu and Benning, 2013). In an effort to understand algal TAG production during N deprivation and to guide engineering of higher oil yields, omics-based approaches have been employed (Jamers et al., 2009). Using the annotated *C. reinhardtii*

[1]This work was supported as part of the Center for Advanced Biofuels Systems, an Energy Frontier Research Center funded by the U.S. Department of Energy, Office of Science, Office of Basic Energy Sciences (award no. DE–SC0001295).

* Address correspondence to yairhill@msu.edu.

The author responsible for distribution of materials integral to the findings presented in this article in accordance with the policy described in the Instructions for Authors (www.plantphysiol.org) is: Yair Shachar-Hill (yairhill@msu.edu).

[OPEN] Articles can be viewed without a subscription.

www.plantphysiol.org/cgi/doi/10.1104/pp.114.250530

genome (Merchant et al., 2007), the *C. reinhardtii* transcriptome was analyzed before and after N deprivation, which revealed multiple changes in gene expression that affect diverse parts of metabolism (Miller et al., 2010; Blaby et al., 2013; Goodenough et al., 2014; Schmollinger et al., 2014). In addition, proteomics have been used to profile the changes in protein expression during N deprivation in *Phaeodactylum tricornutum* (Yang et al., 2014), *C. reinhardtii* (Nguyen et al., 2011; Longworth et al., 2012; Schmollinger et al., 2014), and *Nannochloropsis oceanica* (Dong et al., 2013), and metabolomics have been used to assess changes in metabolite pool sizes (Bölling and Fiehn, 2005; Lee et al., 2012). These and other studies point to wide-ranging changes in the structure and operation of the metabolic and other cellular networks. Several studies have considered the relationships among metabolic processes, including how carbon and energy fixation by photosynthesis affects oil accumulation during N deprivation (Miller et al., 2010; Msanne et al., 2012; Johnson and Alric, 2013). However an integrated systems analysis of both the machinery and the physiological functioning of the photosynthetic apparatus during nutrient deprivation is still lacking, and this limits our understanding of the multilevel regulation of energy and carbon fluxes.

During N deprivation in algae, energy and carbon for de novo synthesis of TAG can come directly from photosynthesis (Msanne et al., 2012) or from external carbon substrates (Wang et al., 2009; Johnson and Alric, 2013). Photosynthetic yields decrease during N deprivation, even under phototrophic conditions where cells are entirely dependent upon photosynthesis (Philipps et al., 2012; Simionato et al., 2013). Chlorophyll (Chl) fluorescence, which is sensitive to environmental changes and stress conditions that induce alterations in photosynthetic components (Iwai et al., 2008), can monitor the efficiency of linear electron flow (Baker et al., 2007) and has indicated that in *N. oceanica* (Simionato et al., 2013) and other algae, including *C. reinhardtii* (Berges et al., 1996; Li et al., 2010; Blaby et al., 2013), photosynthetic efficiency falls after N deprivation. Photosynthetically driven metabolic fluxes can also be probed by supplying ^{13}C-labeled bicarbonate/CO_2 and quantifying ^{13}C incorporation into metabolite pools (Shastri and Morgan, 2007; Feng et al., 2010; Young et al., 2011).

Thylakoid membrane lipids are central to photosynthetic function, including the stabilization of photosynthetic complexes and oxygen evolution (Jarvis et al., 2000; Jones, 2007; Leng et al., 2008; Mizusawa and Wada, 2012; Boudière et al., 2013). The most abundant classes are the neutral lipids monogalactosyldiacylglycerol (MGDG) and digalactosyldiacylglycerol (DGDG) and the anionic lipids sulfoquinovosyldiacylglycerol (SQGD) and phosphatidylglycerol (PG; Frentzen, 2004; Shimojima et al., 2010; Mizusawa and Wada, 2012). Stress, nutrient deprivation, or changing environmental conditions cause changes in lipid composition, leading to effects on photosynthetic yield and efficiency (Li et al., 2012; Philipps et al., 2012). Cellular Chl and carotenoid concentrations provide additional measures of photosynthetic potential. Carotenoids play a role in protecting cells from excess energy harvesting and act as structural components in the photocenters (Takaichi, 2011). In *C. reinhardtii*, decreasing Chl content is associated with down-regulation of synthesis genes and potentially also degradation and follows a decrease in photosynthetic yield during N deprivation (Li et al., 2010; Philipps et al., 2012).

This study examines photosynthetic changes at the level of transcript, protein, lipid, and functional fluxes during the first 48 h after N deprivation. Until recently, studies of nutrient limitation in microalgae have focused on the effects seen one to several days after deprivation (Wykoff et al., 1998; Moseley et al., 2002; Urzica et al., 2013) when oil accumulation rates are high (Plumley and Schmidt, 1989; Li et al., 2010; Miller et al., 2010; Philipps et al., 2012; Simionato et al., 2013; Yang et al., 2013) and photosynthetic functions are already substantially diminished. Here, we focus on the induction phase to investigate the transition into a nutrient-deprived, oil-accumulating state and the regulation of photosynthesis during that transition. The results demonstrate coordinated changes in photosynthetic gene expression as well as the levels of the photosynthetic machinery and their activities. Photosynthetic transcripts, and to a lesser extent protein levels for different parts of the photosynthetic infrastructure, were down-regulated, as were the levels of thylakoid lipids and Chl. Photosynthetic function as measured by dynamic optical parameters indicated modest decreases in the efficiency of light utilization during the first 24 h and a relative decrease in linear compared with cyclic electron flow (CEF). Calvin cycle protein and transcript levels decreased modestly after 6 h, though ^{13}C-labeling incorporation from CO_2 was significantly reduced by that time. The results provide a multilevel description of the controlled down-regulation of photosynthetic components and photosynthetic fluxes, highlight the value of combined multiomic and functional measurements, and have significant implications for current hypotheses about the relationship between photosynthesis and TAG accumulation in algae.

RESULTS

Changes in the Levels of Transcripts and Proteins of Photosynthesis

C. reinhardtii samples were harvested at 0, 0.5, 1, 2, 4, 6, 12, and 24 h after N deprivation, and transcripts were analyzed by high-throughput sequencing as described by Park et al. (2014). Nitrogen-replete cells (time 0) were used as the reference for all subsequent time points. Quantitative proteomic analysis was performed using iTRAQ labeling combined with strong cation exchange fractionation and nano liquid chromatography (nanoLC)-electrospray ionization-tandem mass spectrometry (MS/MS) at all the time points except for 0.5 h. One hundred ninety-two photosynthetically related genes with putative or confirmed annotations were collected using genomic annotation, the literature, and additional databases (see "Materials and Methods"). Genes were

classed as belonging to the following functional groups: photosynthetic-reaction center complexes, light-harvesting complexes, electron transport, photosynthetic antennae, carbon-concentrating mechanisms, the Calvin-Benson cycle, oxidative stress responses, and pigment production and degradation. The transcript and protein level changes for these are presented in Supplemental Figure S1 and Supplemental Table S1. As previously reported, (Merchant et al., 2007; Schmollinger et al., 2014), expression of most photosynthetic genes is down-regulated during N deprivation, with a wide range of trajectories.

To analyze gene expression for different functional groups within photosynthesis in a statistically objective manner, K-means clustering was performed, which divided the transcripts into seven different expression patterns or classes (average, 2.1 within class variance over 50 iterations; Fig. 1A). Agglomerative hierarchical clustering of the expression classes demonstrated four overarching expression trends, with classes 5, 3, 2, and 7 clustering together and classes 6, 1, and 4 by themselves. The distribution of the genes for each functional group across the expression pattern classes (K-means classes) are shown in Figure 1B, and the contribution of genes from each functional group to the different K-means classes is shown in Figure 1C.

The transcript levels for many genes involved in the photosynthetic light reactions decreased within 30 min after N deprivation, continuing to 24 h. There are several notable exceptions, especially those found in expression class 1, including the PSII 22-kDa protein and cytochrome c6, whose transcripts increased in abundance. Additionally, PSII and PSI genes in general appear in two different expression classes, with PSII dominantly in expression class 1, while PSI appears in expression class 6; this difference in photosystem regulation has been found in other organisms (Berges et al., 1996). The decrease in transcript abundance was greatest for three genes corresponding to oxygen evolution enhancers 1 to 3 in PSII and for most genes in PSI, with decreases of the order of 10- to 100-fold. Photosynthetic antenna proteins showed 10- to 20-fold decreases in transcript abundance for both light-harvesting centers1 LHC1 and LHC2 during the first 24 h of N deprivation. LHC stress-related proteins LHCSR1, LHCSR2, and LHCSR3 (class 1), also involved in nonphotochemical quenching (NPQ; Peers et al., 2009; Tokutsu and Minagawa, 2013; Maruyama et al., 2014), increased in protein abundance by 2.5-fold. Transcript abundance for most genes of the Calvin-Benson cycle are found in expression class 1, increasing in the first four and then dropping to the original values or lower by 24 h. Calvin-Benson cycle protein abundances are maintained through 12 h and then decrease slightly by 24 h.

While PSI and PSII genes were down-regulated, genes implicated in both CEF pathways were up-regulated. In the Proton Gradient Regulation5 (PGR5)-mediated pathway, PGR5 and Proton Gradient Regulation-Like1B (PGRL1B), both found in green algae and higher plants, aid transfer of electrons from reduced ferredoxin to plastoquinol (Munekage et al., 2002; Petroutsos et al., 2009; Hertle et al., 2013; Johnson et al., 2014). These genes both doubled in transcript abundance within 1 h, with levels falling to N-replete levels by 24 h, similar to values reported in Schmollinger et al. (2014); protein levels were not reliably quantified. PGRL1 was also found to respond to iron deficiency (Petroutsos et al., 2009). A type 2 NADPH Dehydrogenase NDA2 is thought to be responsible for the second CEF pathway in *C. reinhardtii* (Jans et al., 2008; Johnson et al., 2014). NDA2 transcript abundances increased slightly by 24 h, while protein level increased 1.5-fold by 24 h, suggesting that CEF through this route may increase during N deprivation.

Carbon concentrating mechanism-related genes (for review, see Wang et al., 2011), such as the carbonic anhydrases CAH1 (Van and Spalding, 1999) and CAH3, and carbon limiting-associated genes Carbon Concentrating Protein1 (CCP1), CCP2, Low Carbon-Induced E (LCIE), and LCI9 showed increased transcript abundance in the first 4 h, which then decreased, represented by expression class 1, while protein abundance increased by 24 h. This was likewise found in the marine alga *Dunaliella tertiolecta* 'Butcher' (Young and Beardall, 2005) and *Chlorella* spp. (Beardall et al., 1982; Beardall et al., 1991), where both Fe and N limitation led to an increased affinity for inorganic carbon. Others such as CAH2 showed a decrease in transcript expression over time (class 7). CAH1 and similar proteins have been found in the periplasm and growth medium under ambient-air CO_2 concentrations (Coleman et al., 1984).

Genes involved with removing radical oxygen species such as Iron Superoxide Dismutase1 (Myouga et al., 2008) and Catalase1 (Yoshida et al., 2003) showed declines in transcript and protein levels. An exception is GPX5 (a glutathione peroxidase), whose transcript levels increased by approximately 30% by 24 h of deprivation and whose protein abundance increased approximately 20%. GPX5 is known to metabolize peroxide, and like other oxidative stress response genes, is known to be up-regulated under photosynthetic stress conditions such as high light (Fischer et al., 2009). Protein levels followed transcript changes 6 to 12 h after N deprivation.

Questions have been raised about the importance and mechanisms of alternative electron acceptor pathways, such as chlororespiration, in regulating photosynthetic energy fluxes during N deprivation (Peltier and Schmidt, 1991). The alternative oxidases, plastid plastoquinol terminal oxidases PTOX1 and PTOX2, are thought to be involved in the chlororespiration in *C. reinhardtii* (Rumeau et al., 2007; Bailleul et al., 2010; Houille-Vernes et al., 2011), and changes in protein and transcript abundance have been found to be associated with nutrient deprivation in algae, particularly iron deprivation (Cardol et al., 2008) as well as light stress (Houille-Vernes et al., 2011). PTOX1 and PTOX2 transcripts decreased in abundance 1.5-fold within the first half hour but then increased through 24 h to slightly less or greater than N-replete conditions.

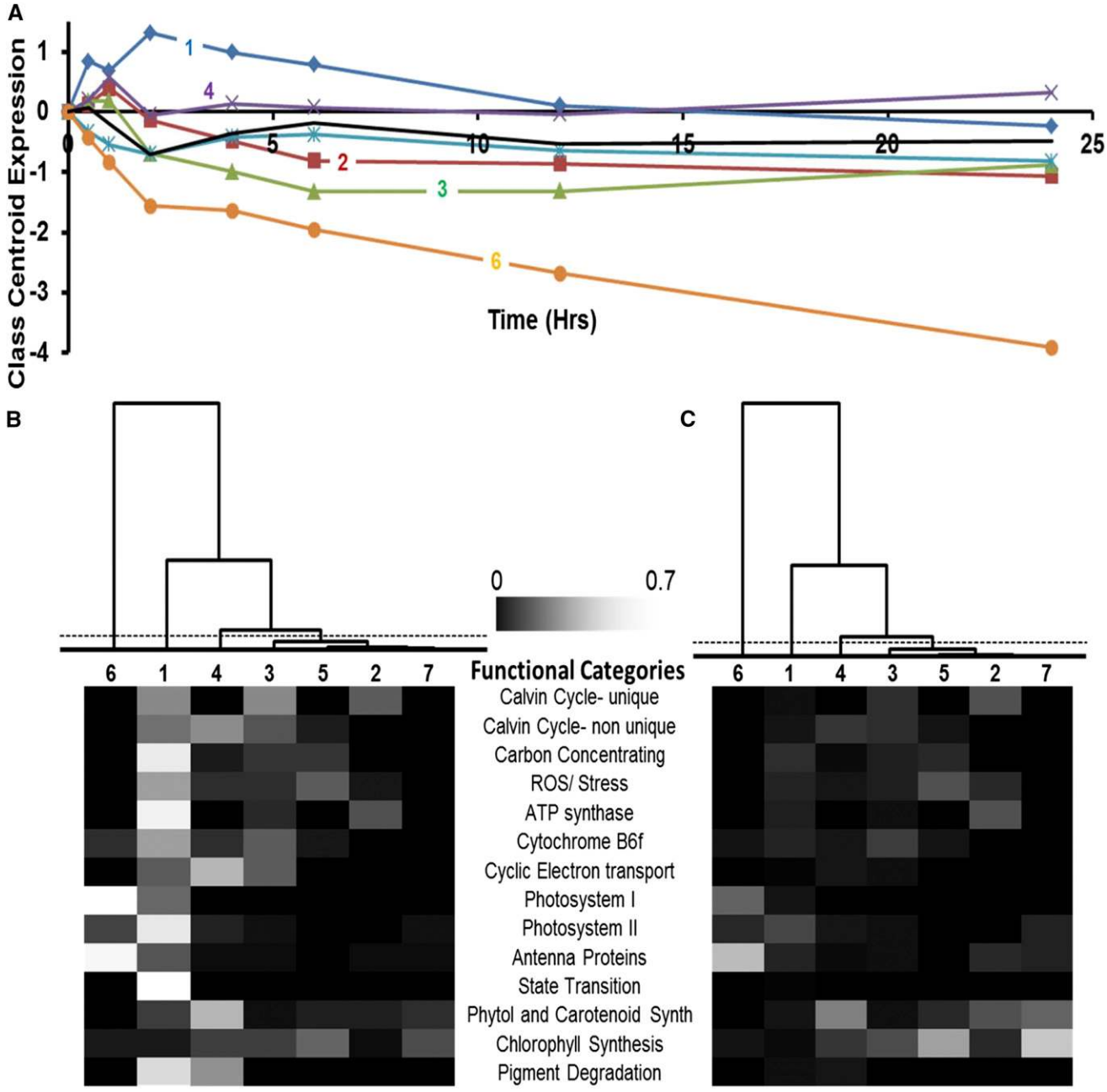

Figure 1. Statistical analysis of photosynthetic transcripts. A, K-means clustering class centroid expression (log fold change [$\pm$ $\log_2$]) of classes derived from statistical analysis. Blue diamond, Class 1; red square, class 2; green triangle, class 3; purple X, class 4; teal star, class 5; orange circle, class 6; and black cross, class 7. B and C, Heat maps of class fractional enrichment by functional group member totals (row total normalized to add to 1) and class member totals (column total normalized to equal 1). Member enrichment is indicated by black, while enrichment of 0.7 or more is indicated by white. Gene functional categories are listed between B and C. Dendrograms above B and C heat maps represent statistical difference between each expression class in A, while numbers indicate class number being presented.

PTOX2 protein values increased 2.4-fold by 24 h, suggesting that during N deprivation, in addition to linear and cyclic electron transport being down-regulated, additional electrons are returned to oxygen, which may help to regulate the ATP to NADPH ratio and photosynthetic output (Peltier and Schmidt, 1991). This may help explain why we observed only minor decreases in the oxidation level of PSII primary quinone A (Q_A; Fig. 4D).

Pigment Levels and Their Regulation

Chl content decreased during N deprivation, with levels dropping from approximately 33 μg mg^{-1} cell

dry weight (CDW) to less than 10 μg mg^{-1} CDW after 24 h of N deprivation (Fig. 2A), with decreases being most rapid soon after deprivation. Chl content per million cells (Fig. 2B) fell from 0.9 to 0.63 μg within the first 12 h and then declined more slowly to 0.43 μg by 48 h. The ratio of Chl *a* to Chl *b* was not significantly altered. However, Figure 2B shows that Chl levels per culture volume were initially unchanged after N deprivation and decreased rather slowly after 6 h.

Chl synthesis genes for both the porphyrin ring and phytol chain were rapidly down-regulated at both the transcript and protein levels, with transcripts falling by one-half and proteins by approximately 30% of initial values by 2 h, while transcript abundances for Chl catabolic genes, such as chlorophyllase, were significantly elevated after 1 h. ^{13}C labeling and analysis of phytol ^{13}C contents was therefore used to follow Chl synthesis rates during N deprivation (Fig. 2C). N-depleted cells supplied with ^{13}C acetate incorporated ^{13}C into Chl or phytol only within the first 3 h, indicating that de novo Chl synthesis ceases soon after N deprivation. This cessation of synthesis, together with the continued growth (cell division continued for 12 h after N deprivation substantial rates of biomass increase continued beyond that), is sufficient to account for the large decreases in Chl content over the first 24 h without significant Chl degradation. It has been suggested that Chl decreases following N deprivation in cyanobacteria are due to dilution from cell growth (Collier and Grossman, 1992), which we demonstrate here with ^{13}C labeling. Chl degradation has been previously inferred to occur both to remobilize nitrogen (from both Chl and associated proteins) and to reduce light stress (Allen and Smith, 1969; Geider et al., 1998).

Carotenoids are involved with light absorption and energy dissipation, reducing radical oxygen species production (Lohr, 2009). Within the first 4 h of N deprivation, the expression of some carotenoid synthesis and modification genes were strongly up-regulated, while most stayed at the same level or decreased. After 4 h, most of the related transcript abundances decreased, although they were still elevated compared with N-replete conditions. Transcript levels of the degradation enzymes carotenoid cleavage dioxygenases CCD1 and CCD2 were elevated during N deprivation. Carotenoid levels, determined by HPLC at 450 nm (Supplemental Fig. S2, A–F), showed that levels of the xanthophyll cycle carotenoid violaxanthin (Jahns and Holzwarth, 2012) decreased continuously, being undetectable by 48 h, while zeaxanthin levels doubled by 24 h relative to time 0-h levels and then returned to initial levels at 48 h after N deprivation. Levels of other xanthin carotenoids, neoxanthin and loraxanthin, and lutein also decreased after N deprivation, with neoxanthin falling to undetectable levels after 48 h of deprivation. β-Carotene levels showed a trend similar to free zeaxanthin, with an increase to 24 h and then a decrease back to initial values at 48 h.

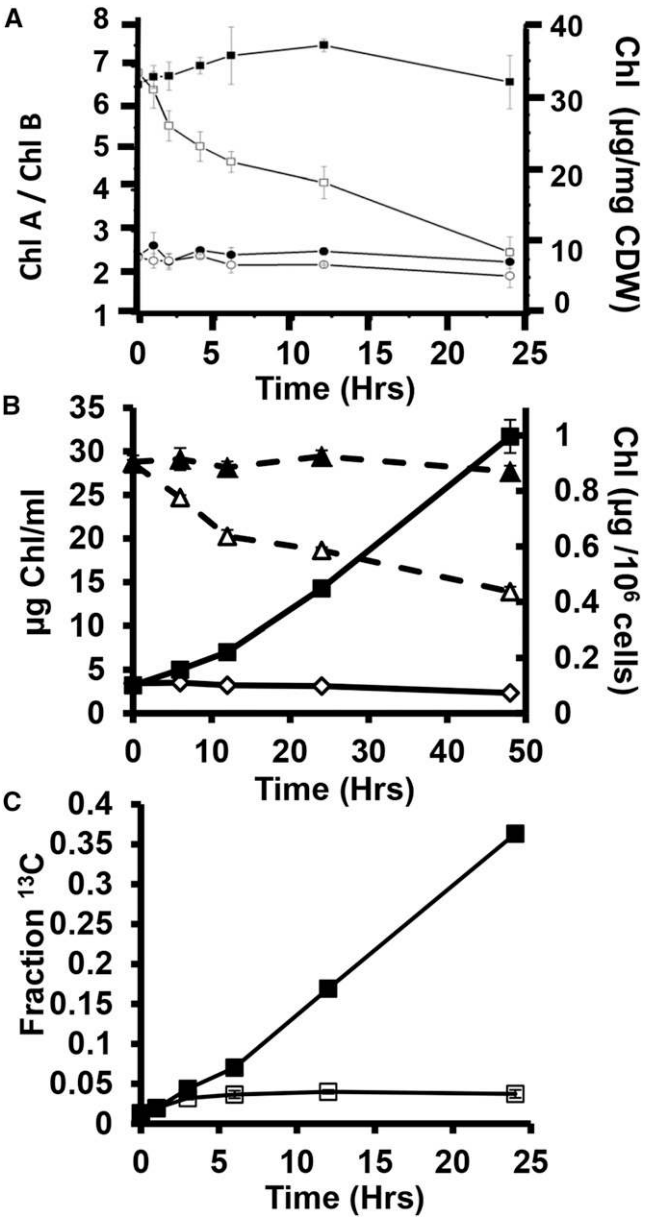

Figure 2. Chl concentrations and synthesis. A, Chl concentration per CDW in N-replete and N-depleted cultures (black and white rectangles, respectively). The ratio of Chl *a* to Chl *b* for N replete and N depleted (black and white circles, respectively). B, Micrograms of Chl per culture volume of N replete (black square) and N deplete (white square). C, ^{13}C incorporation in molecules containing ^{13}C label in N-replete and N-depleted cultures (black and white rectangles, respectively). Error bars indicate SD (n = 3).

Thylakoid Lipid Levels and Composition

Over the course of N deprivation, we observed a decrease in the levels of thylakoid membrane lipids. This includes the glycolipids MGDG and DGDG and the anionic lipids SQGD and PG (Benning, 2010; Shimojima et al., 2010). There was a sharp decrease in their levels in the first 6 h and then a more gradual decrease until 24 h

(Supplemental Fig. S3). Proportions of polar (PG and SQGD) and nonpolar (MGDG and DGDG) thylakoid lipid levels did not change, which suggests that the thylakoid membrane composition and charge density are maintained. Thylakoid structure was examined by electron microscopy during the first 48 h of N deprivation (Fig. 3), revealing that the chloroplast decreases in size, consistent with the decreases observed in plastid membrane lipid levels. Thylakoid stack structure appears normal until at least 72 h, which contrasts with the deterioration of cytosolic structure and suggests that photosynthetic capacity is maintained.

Energy Capture and Conversion Is Down-Regulated during N Deprivation

We used Chl fluorescence spectroscopy to assess photosynthetic function during N deprivation. Over the 48-h N deprivation time course, a slow, approximately linear decrease in the theoretical maximum quantum efficiency of PSII (F_v/F_m; Baker, 2008) occurred. After 24 h, F_v/F_m was approximately 85% of N-replete values, and at 48 h, it was approximately 75%, similar to the levels reported by Schmollinger et al. (2014) and (Li et al. (2010). The operating quantum efficiency of PSII photochemistry in the light (Φ_{II}; Genty et al., 1989; Baker, 2008) decreased continually after 6 h, reaching close to one-half the initial value by 48 h (Fig. 4B). In N-replete cells, Φ_{II} was 15% lower than the F_v/F_m, while N-deprived Φ_{II} was almost 55% lower. NPQ during N deprivation was also measured (Fig. 4C), showing that in N-deprived cells, NPQ decreased from approximately 0.3 to approximately 0.07 by 48 h.

In PSII, the efficiency of electron transfer is partly dependent on the number of open/oxidized Q_A. qP and qL are two parameters used to describe the percentage of open PSII reaction centers (oxidized Q_A pool) based on the puddle (qP) and lake (qL) models, respectively (Kramer et al., 2004). During N deprivation, qP fell from 0.93 to 0.82 in 6 h and further to 0.75 by 48 h, indicating a decrease in the abundance of open reaction centers, while in N-replete control cultures, its levels remained constant throughout the time course (Fig. 5D). qL is similar to qP, except that it takes in to account the lake model of shared light-harvesting centers. In these experiments, its values were approximately 1% to 2% lower than qP. Both qP and qL demonstrated that the Q_A pool was increasingly reduced over time (Supplemental Fig. S4).

To probe potential changes in the allocation of light energy between photosystems, 77-K fluorescence spectra, which are a measure of the amount of light-harvesting complex Chl associated with different photocenters, were acquired (Fig. 4E). A substantial fall in the fluorescence peak at 715 nm relative to the PSII peak at 685 nm was observed at 6 h and beyond (consistent with previous

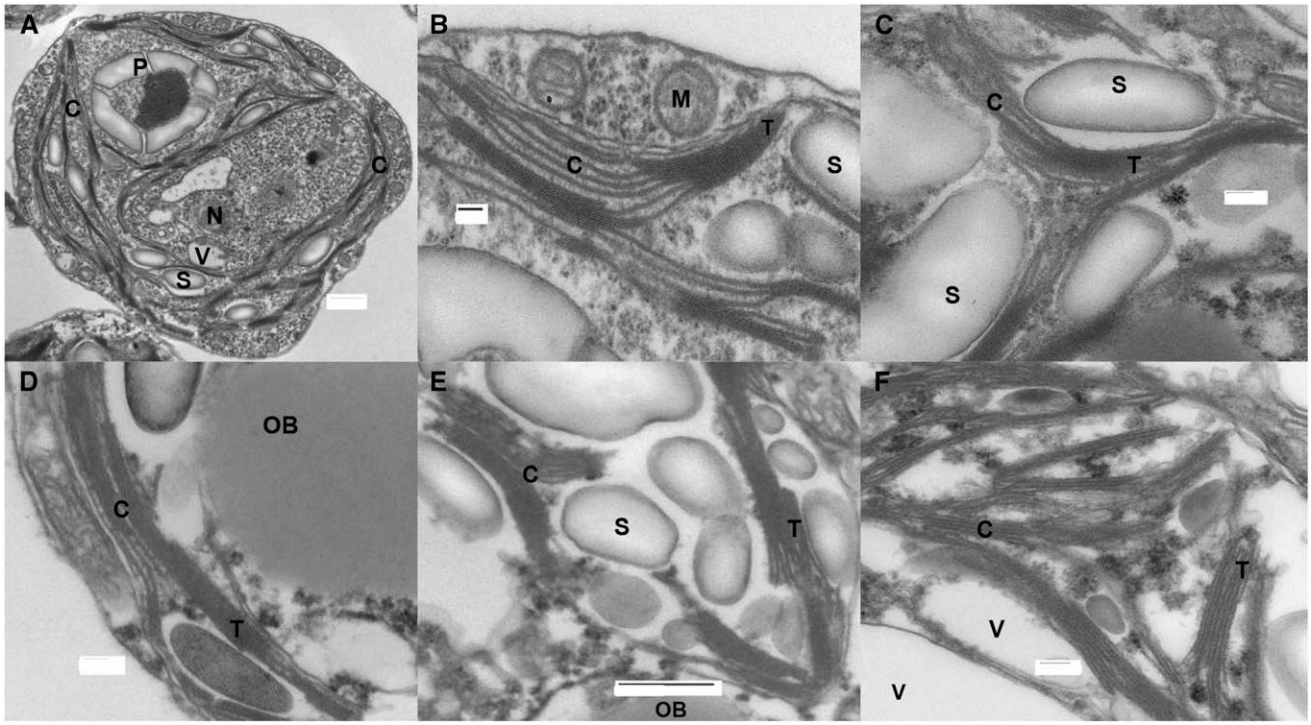

Figure 3. Chloroplast imaging with electron microscopy. A, N-replete cell. B, N-replete chloroplast. C, Six-hour N-depleted chloroplast. D, Twelve-hour N-depleted chloroplast. E, Twenty-four-hour N-depleted chloroplast. F, Forty-eight-hour N-depleted chloroplast. Bars = 500 nm (A and E) and 100 nm (B–D and F). C, Chloroplast; M, mitochondria; N, nucleus; OB, oil bodies; P, pyrenoid; S, starch; T, thylakoids; V, vacuole.

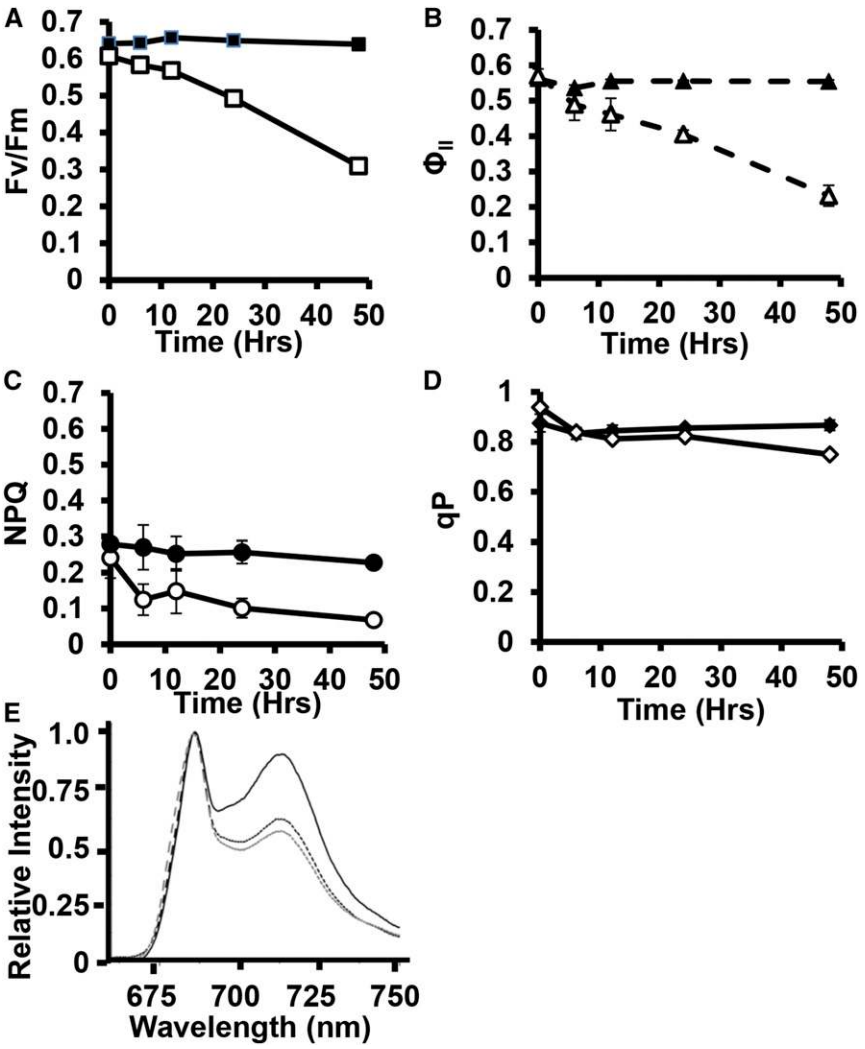

Figure 4. Photosynthetic fluorescence functional measurements. A, F_v/F_m. B, Φ_{II}. C, NPQ. D, qP. E, 77-K fluorescence. Contributions to efficiency decreases were measured through Chl fluorescence experiments over 48 h of N deprivation using PAM fluorometry. A to D, Black shapes indicate N replete and white shapes indicate N-depleted conditions. E, 77-K fluorescence spectra during N deprivation. Control (black line), 6-h N depleted (black hashed line), and 24-h N depleted (gray hashed line) are shown. PSI-associated fluorescence (maximum at 715 nm) decreased markedly from 95% to 65% (±1%) of the fluorescence intensity at PSII (maximum at 685 nm) by 6 h and then decreased slightly (58% ± 7%) by 24 h. Not shown are 48- and 72-h curves, which had fluorescence signals at 715 nm, with 64% and 66% (±3%), respectively, of the signal intensity at 685 nm. Error bars indicate SD ($n = 3$). Each 77-K spectrum is the average of three replicates.

reports in nitrogen-limited *C. reinhardtii*; Plumley et al., 1989). State Transition7 (class 1), a protein kinase responsible for inducing state transitions and adaptation to different light conditions (Depége et al., 2003), increased 3-fold in transcript abundance within 2 h and then returned to initial levels by 24 h, while its protein levels decreased from 6 to 24 h. 77-K spectra and protein data suggest a decreasing role for state transitions during N deprivation. Alternatively, the 77-K spectra could represent rapid remodeling of antennae and photocenter arrangements.

Oxygen Evolution

Photosynthetic oxygen evolution in the light and its consumption immediately upon transfer to the dark were measured over the N-depleted time course (Fig. 5A). Under the growth conditions of this study (160 uE m^{-2} s^{-1}), light-driven gross oxygen evolution and consumption rates per cell decreased by one-half in the first 12 h, with minor decreases through 48 h. Similar trends in oxygen exchange rates were recently reported by Schmollinger et al. (2014) using higher light levels for measurement than for culturing. Thus, the electron flux through PSII was down-regulated over the first 24 h after nitrogen deprivation, and this can be accounted for by the measured decreases in the efficiency of PSII and Chl levels.

Total PSI Turnover Rate Falls during N Deprivation

The absorbance changes at 705 nm under PSII-inhibited conditions are proportional to the oxidation/reduction of PSI (Alric, 2010; Johnson and Alric, 2012). These P700 absorbance changes shown in Figure 5 are attributed to redox turnover at PSI due to CEF (Fig. 5B). Thus, CEF rates fall by approximately 50% over 48 h when expressed on a per cell basis; when expressed on a per Chl basis, the decreases are more modest. This indicates that cellular rates of CEF fall more because of decreases in the numbers of photocenters per cell (as reflected in Chl levels) than because of the turnover rates of each photocenter.

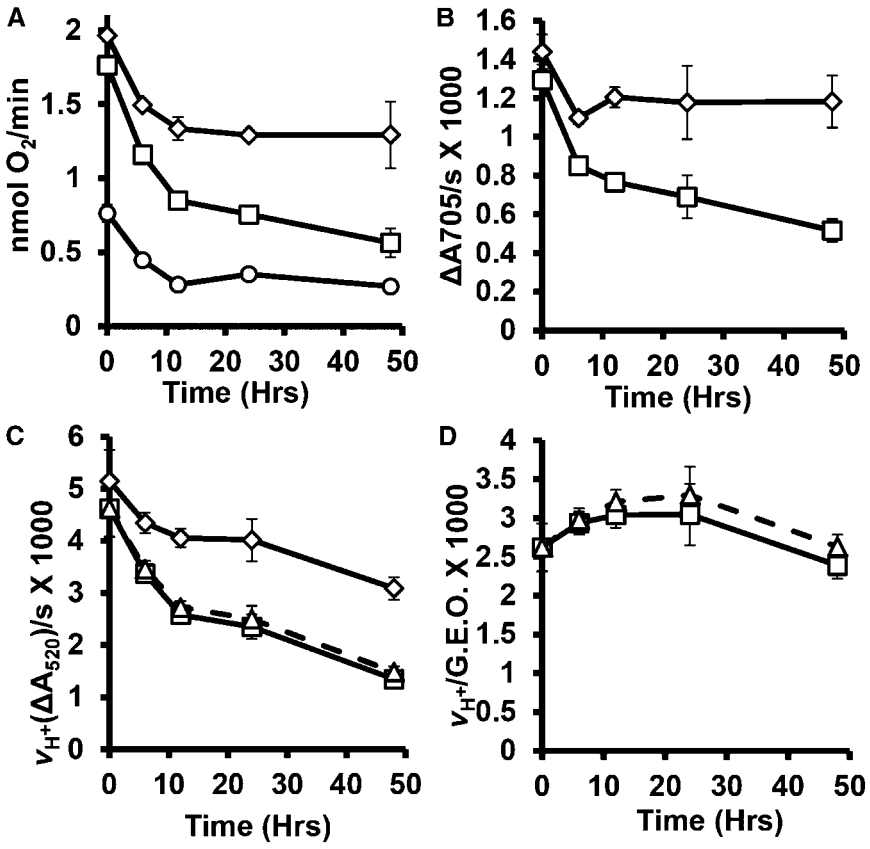

Figure 5. Oxygen evolution, ECS, and P700 spectroscopy. A to C, White squares indicate values per million cells and white diamonds indicate values per microgram Chl. A, Gross oxygen evolution and consumption (white circle; nmol min^{-1}). B, P700 (ΔA_{705} s^{-1}) × 1,000. C, ν_{H^+} (ΔA_{520} s^{-1}) × 1,000. White triangle and dashed line indicate samples normalized to PSII-inhibited P700/ECS ratios. D, ν_{H^+}/GEO × 1,000. White square and black line show ν_{H^+}/GEO values and white triangles and dashed line show ν_{H^+}/GEO values normalized to PSII-inhibited P700/ν_{H^+} ratios. Error bars indicate SD (n = 3).

Electrochromic Shift Measurements to Probe Thylakoid Proton Motive Force and Fluxes

The electrochemical potential across thylakoid membranes was assessed using electrochromic shift (ECS)-induced absorbance changes at 520 nm (Avenson et al., 2005; Bailleul et al., 2010; Lucker and Kramer, 2013). When pigments are immobilized within an electric field, a shift in the dipole moment can be induced, which changes the spectral properties of the pigment absorbance. Changes in absorbance at 520 nm during brief periods of dark are due to the dissipation of the thylakoid proton motive force. This is believed to occur primarily through proton translocation through the ATP synthase. The initial slope of ECS-induced absorbance change during light-to-dark transitions gives estimates of total proton efflux (ν_{H^+}) during steady-state photosynthesis. Figure 5C shows that ν_{H^+} decreased by approximately 50% in the first 12 h after N deprivation and then another 20% by 48 h.

The amplitude of the ECS signal is proportional to the concentration of the relevant pigments and the amplitude of the electrochemical potential. Therefore, to account for any changes in pigment concentrations on the ν_{H^+} calculation during the N-deprived time course, we normalized the ECS signal using the P700 absorbance changes in the presence of 3(3,4-dichlorophenyl)-1,1-dimethylurea. This was rationalized as follows. Under PSII-inhibited conditions, changes in A_{705} during light-to-dark transitions are directly proportional to PSI turnovers under PSII-inhibited conditions and are linearly proportional to the ECS at 520 nm signal (Lucker and Kramer, 2013). We can therefore calibrate changes in the ECS signal due to pigment changes with the PSI signal. The PSII-inhibited Δ705 to Δ520 nm ratio (Supplemental Fig. S5) was found to increase only approximately 10% by 48 h, demonstrating that pigment changes had minimal impact on measured ECS absorbance changes over the time course. This is consistent with the observation that carotenoid pigment levels change much less than Chl, and it allows greater confidence in the estimates of proton flux. Normalized ν_{H^+} is presented in Figure 5C.

To determine the relative contributions of linear electron flow (LEF) and CEF to total photosynthetic electron flow, we compared ν_{H^+} to gross evolved oxygen (GEO) rates during nutrient deprivation. Figure 5D shows that during N deprivation, ν_{H^+}/GEO increases approximately 15% by 24 h, indicating modest increases in the contribution of CEF relative to LEF to the chloroplastic proton motive force. From 24 to 48 h, ν_{H^+}/GEO decreased to N-replete levels. Calibrated ν_{H^+}/GEO shows a small increase in favor of CEF versus LEF over the time course, most significantly at 24 h.

Photosynthetic Carbon Fixation

Steady-state ^{13}C-labeling experiments showed that under nutrient-replete conditions, photosynthetic carbon

fixation contributed approximately one-third of carbon used for growth. To assess changes in flux from photosynthetic carbon fixation into soluble metabolite pools, cells were pulse labeled with ^{13}C bicarbonate before or 6 h after N deprivation (Fig. 6). The rate of labeling of Glc-6-P and particularly of Gly and Ser was reduced by between 15% and 50% within 6 h of N deprivation, indicating that fluxes through the photosynthetic dark reactions of the Calvin cycle are substantially reduced before any significant changes in the relevant enzyme levels.

Starch Synthesis

In *C. reinhardtii*, N deprivation induces the accumulation of starch sooner and to a greater extent than TAG (Siaut et al., 2011; Fan et al., 2012). Starch levels (Fig. 7A) show a linear increase starting within 6 h and increasing from 5 μg per million cells to approximately 25 μg per million cells by 48 h. Transcripts for genes related to starch synthesis (Fig. 7B; Supplemental Table S1), especially soluble starch synthase I, are up-regulated within 30 min of N deprivation, while most genes related to starch degradation were down-regulated early on. The levels of most of the corresponding proteins closely followed changes in transcripts. Interestingly, the expression of some starch degradation genes, including many starch-binding and -debranching enzymes, are up-regulated after 4 h. Such findings suggest that the starch pool may be turned over during N deprivation, which would point to starch metabolism having more than a simple storage function. Starch turnover has been demonstrated during normal growth (Klein, 1987) and has been suggested to occur during N deprivation based on observations on starch-breakdown mutants (Tunçay et al., 2013). Starch accumulation occurs during a time when cells are down-regulating photosynthesis, decreasing carbon fixation, and reducing ATP and NADPH production. While oxygen production rates before N deprivation are sufficient to sustain the initial starch accumulation rates, within approximately 12 h, this is no longer the case, and we therefore suggest that starch accumulation is not primarily driven by photosynthetic carbon or energy overflow under these conditions.

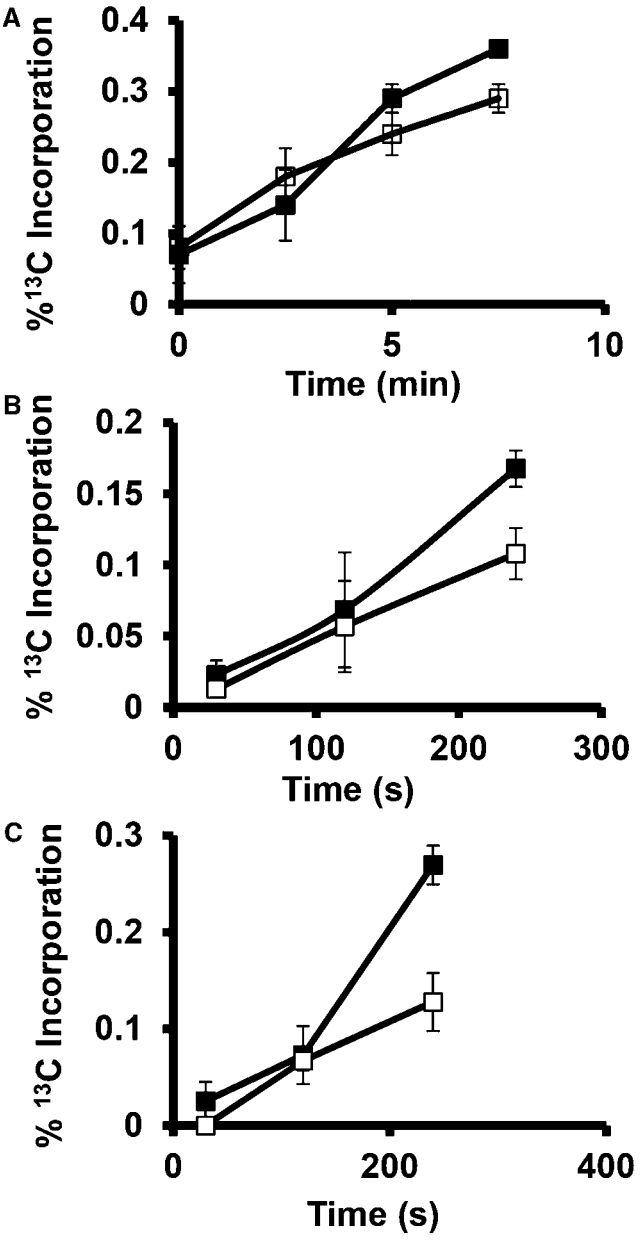

Figure 6. ^{13}C incorporation. Time course of ^{13}C incorporated into Glc-6-P (A), Gly (B), and Ser (C) after addition of ^{13}C bicarbonate to cultures deprived of N for 6 h. The percentages of molecules containing ^{13}C label were determined by GC/MS after rapid quenching of cells in –70°C methanol and subsequent extraction. Error bars indicate SD (n = 3).

DISCUSSION

Regulation of Photosynthetic Activity

When microalgae are deprived of nitrogen or other inorganic nutrients, growth slows, photosynthesis is down-regulated, and starch and oil accumulate. Pronounced and rapid decreases in transcripts for most genes encoding the photosynthetic complexes, electron transport, light-harvesting centers, photosynthetic pigments, and the Calvin-Benson cycle were observed here and in other studies (Miller et al., 2010; Blaby et al., 2013; Schmollinger et al., 2014), pointing to a central role for transcriptional regulation in reducing photosynthetic rates. Protein levels for many of these genes also decreased, albeit to a substantially lesser extent and with delays generally in the 6- to 12-h range. However, analyses of photosynthetic energy fluxes and of ^{13}C-labeling rates show that regulation at the posttranslational level is at least as important as expression changes in the short-term response to nutrient deprivation. Thus photosynthetic CO_2 fixation and Chl synthesis rates are both markedly inhibited before the corresponding protein

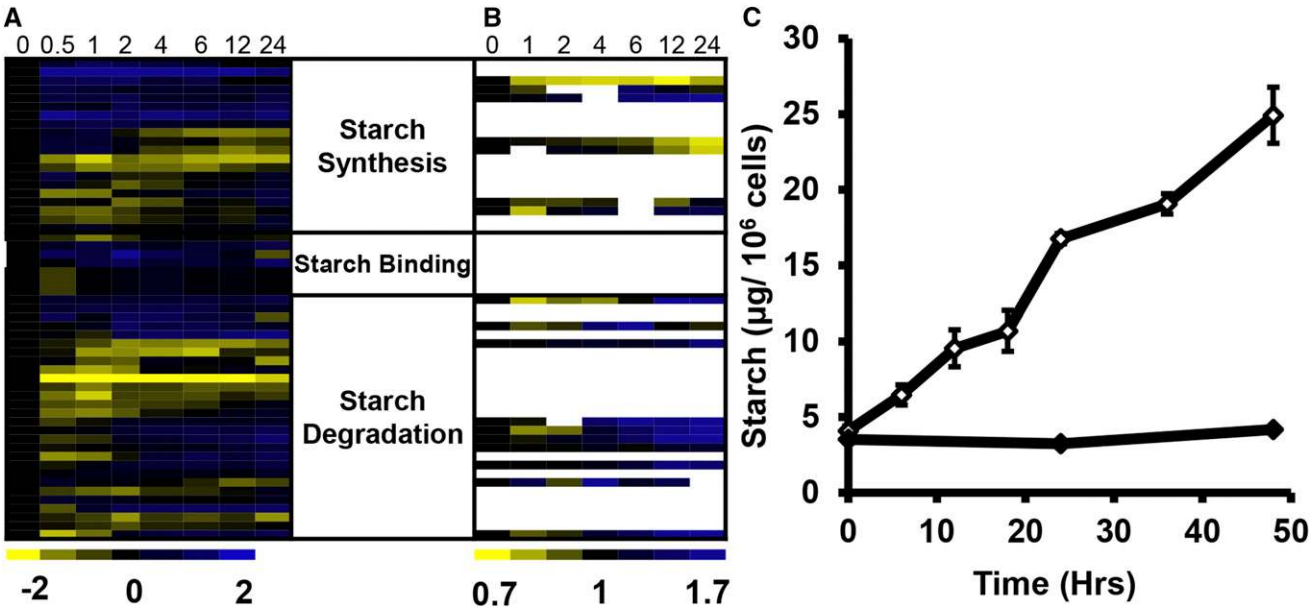

Figure 7. Starch analysis. Transcripts (A) and protein (B) abundance values over a 24-h N-depleted time course for genes related to starch metabolism. Transcript values are expressed as $\log_2$-fold change, and protein values are expressed as ratios of value at time point to original value at time 0; each follows the color scales denoted below their respective sections, with blue representing an increase in expression, yellow representing a decrease, and white representing not reliably quantified. C shows starch levels in N-replete (black diamonds) and N-deprived (white diamonds) cells. Error bars indicate SD (n = 3).

levels are significantly decreased. Likewise, the timing of changes in the photosynthetic apparatus and in electron and proton fluxes does not correlate with the expression levels of the relevant genes. For example, as a whole, expression of almost all PSI genes are decreased relative to that of PSII genes, whereas CEF fluxes at PSI increase relative to LEF, which are initiated at PSII. Another significant posttranslational change is the relative partitioning of light-harvesting complexes between the photosystems, which occurs within 6 h, before the levels of the antennae proteins have changed significantly. Posttranslational regulation of photosynthesis is known to be important in a range of stress responses as well as in diurnal changes (de Vitry et al., 1989; Geiger and Servaites, 1994; Turkina et al., 2006; Pfalz et al., 2012). Such changes include structural modifications of individual proteins and photosynthetic complexes as well as allosteric regulation of enzyme activities.

Differential Regulation of PSI and PSII

It has been reported that PSI and PSII respond quite differently during N deprivation, with PSII protein and activity decreasing more than that of PSI (Plumley et al., 1989; Berges et al., 1996; Wykoff et al., 1998). Plumley et al. (1989; in *C. reinhardtii*) and Berges et al. (1996; in *Thalassiosira weissflogii*, *D. tertiolecta*, and *Synechococcus* sp. PCC 7002) concluded that the major effects of nitrogen deprivation are in PSII and that there is a relatively large capacity for CEF under these conditions. Similarly, Wykoff et al. (1998), studying *C. reinhardtii* under S and P deprivation, found that electron flow was inhibited at PSII, whereas PSI activity was essentially unchanged in starved cells. By using multiple measurement methods to assess photosynthetic fluxes, we conclude that under the culture conditions used, fluxes through the two photosystems are both reduced and that while linear electron fluxes fall more than cyclic ones in the first day of nutrient deprivation, the difference is much less dramatic than previously concluded.

At the transcript level, PSII gene expression is increased within 2 h of N deprivation (class 1), while PSI transcript levels fall (class 6). This suggests that PSII protein levels should stay higher longer than PSI; however, this is not the case. Second, from 77-K fluorescence data, we find a higher proportion of Chl fluorescence associated with PSII than PSI over time, which is the reverse of findings in *N. oceanica* (Simionato et al., 2013). By contrast, the gross oxygen evolution rate, a measure of PSII activity, decreases somewhat more than the ν_{H^+} during the first 24 h, indicating a decrease in the contribution of LEF compared with CEF. From 24 to 48 h, there appears to be a rebalancing of photosynthetic electron fluxes, with LEF increasing relative to CEF. Interestingly, F_v/F_m does not decrease rapidly, suggesting that PSII complexes remain functional and that LEF is being down-regulated in another manner partly due to dilution of Chl per cell. As mentioned above, the PTOX protein abundance increases and may be involved in redirecting electrons from linear electron transport toward chlororespiration (Peltier and Schmidt, 1991), while the increases in PGR5, PGRL1B, and NDA2 transcript and protein levels suggest increased CEF capacity (Johnson et al., 2014). The increase over the

first 24 h of the proportion of proton efflux apparently driven by CEF implies there is an increase in demand for photosynthetically generated ATP relative to NADPH. We postulate that such a shift reflects a decreasing demand for NADPH for de novo biosynthesis as growth slows, while ATP demands for maintenance and remodeling of the proteome remain closer to those during normal growth.

Photosynthesis Is Down-Regulated in a Controlled and Orderly Manner

During N deprivation, it has been suggested that photosynthesis induces significant stress via energetic overflows, leading to potential oxidative damage and driving starch and oil accumulation as energy sinks (Roessler, 1990; Hu et al., 2008; Li et al., 2012). Consistent with this, GPX5, a gene associated with reactive oxygen species (ROS), was up-regulated. The photosystem II subunit S (PSBS) gene, believed to be involved in NPQ (Bonente et al., 2008; Miller et al., 2010), the LHCSR genes, and the PSBA D1 protein are also up-regulated, and zeaxanthin levels doubled within 6 h. While zeaxanthin accumulation and LHCSR and PSBS up-regulation are typically associated with light-induced stress and thylakoid acidification (Gilmore and Yamamoto, 1993; Horton et al., 1994; Peers et al., 2009), our other results provide evidence that photosynthetic fluxes are down-regulated sufficiently to prevent significant stress. NPQ, which is elevated markedly under photosynthetic stress conditions such as drought or high light exposure (Niyogi et al., 1997; Müller et al., 2001), did not increase following N deprivation. It may be that the moderate light levels at which *C. reinhardtii* is cultured and at which NPQ was measured here are too low to induce significant quenching. Also, we observed little or no increase in the levels of ROS-related proteins (with the exception of modest increases in GPX5), which is consistent with a recent study in which no increases in ROS levels were detected during N deprivation in wild type *C. reinhardtii* (Li et al., 2012). Chl levels per cell decrease strongly, and this, together with changes in photosynthetic light use efficiency, can be estimated to reduce energy capture by approximately 3-fold within 24 h, consistent with the observation of strong reduction in the light-driven oxygen production rate. It is likely that during the first 24 h, decreased light capture is a more important factor than changes in Calvin cycle enzyme levels or activities in the decreased carbon fixation rates. Also consistent with a picture of an orderly down-regulation of photosynthesis that preserves structure and function while avoiding stress from energy overflow are the findings that Chl levels fall by dilution without the induction of degradation, and the same apparent pattern in the decreasing levels of thylakoid membranes, with their proportions and organization in the thylakoid stacks being preserved. The fact that starch and later TAG accumulation increase while photosynthetic energy capture is greatly decreased suggests that photosynthetic energy overflow may not be the primary driver of storage compound accumulation. Thus, for example, maximal starch production rates are achieved before growth rates have slowed significantly. A full energetic and carbon balance under autotrophic as well as mixotrophic conditions would be needed to quantitatively assess the contribution of photosynthesis to storage compound accumulation. As algae in nature commonly face nutrient deprivation (Grossman, 2000; Grossman et al., 2010; Merchant and Helmann, 2012), it should perhaps not be surprising that they are able to respond in an orderly manner, preventing substantial energetic overflows and oxidative damage.

MATERIALS AND METHODS

Culturing

Chlamydomonas reinhardtii strain cc400 cw-15 mt++ was obtained from the *Chlamydomonas* Research Center and grown at 23°C in liquid Tris-acetate-phosphate (TAP) mediim (Gorman and Levine, 1965) in flasks shaken at 125 rpm under continuous illumination at 160 μE m^{-2} s^{-1} and ambient CO_2 concentrations. Cell growth was determined by optical density measurements at 750 nm using a DU 800 spectrophotometer (Beckman-Coulter). Cultures were grown to cell densities of between 0.15 and 0.3 optical density to minimize self-shading, which becomes significant in denser cultures. Cells were counted using a Z-series Coulter Counter cell and particle counter (Beckman-Coulter). For N deprivation, cells were centrifuged and resuspended in TAP medium lacking ammonium chloride (nitrogen source). For labeling studies, acetate was replaced with $^{13}C_2$ acetate.

Transcriptomics

Transcript analysis was conducted as described in Park et al. (2014), which includes the mapping, parameters for single nucleotide polymorphism analysis, statistical data tools, and functional annotations. Briefly, cells were harvested by centrifugation at 0°C, resuspended in RNAlater solution (Qiagen Sciences), and stored at between –80°C and –60°C ; RNA was extracted from two biological replicates for each time point using TRIzol reagent (Invitrogen) according to the manufacturer's protocol. Complementary DNA library preparation and high throughput RNA sequencing analyses were performed as previously described by He et al. (2012).

Proteomics

Cells were harvested by centrifugation and frozen in liquid N. Proteins were extracted and trypsin digested as described in Wang et al. (2012). One hundred micrograms of each digested sample was labeled using 4plex iTRAQ reagents according to the manufacturer's instructions (AB Sciex). Two 4plex iTRAQ experiments were performed for each biological replicate of the seven time points. Labeled samples from each experiment with iTRAQ labels 114 to 117 were mixed and fractionated via strong cation exchange as in Alvarez et al. (2011). Fractions from 5 to 24 min were analyzed by nanoLC-tandem mass spectrometry (MS/MS) using an LTQ-Orbitrap Velos mass spectrometer (ThermoFisher) coupled with a nanoLC Ultra (Eksigent). Mascot Distiller version 2.4 (Matrix Science) was used to process data, and Mascot Daemon was used to search data against the *C. reinhardtii* protein database from Phytozome9 and the *Chlamydomonas* chloroplast and nuclear database from NCBInr (Phytozome 9, January 7, 2013, 17,114 sequences and 12,173,409 residues). The false-positive rate of protein identification was assessed with an automatic decoy database search, and identified proteins were grouped based on 98% homology with Scaffold version 3.1 (Proteome Software). Full details can be found in Park et al. (2014).

Annotation and Expression Analysis

Transcripts and proteins identified during sequencing were filtered for relatedness to photosynthetic function based upon annotation in Phytozome, Kyoto Encyclopedia of Genes and Genomes, the *C. reinhardtii* sourcebook

(Harris et al., 2008), similarity to Arabidopsis (*Arabidopsis thaliana*) sequences provided on The Arabidopsis Information Resource, and papers cited in this work. K-means and hierarchical clustering for transcripts was carried out using XLSTAT (Addinsoft) in Microsoft Excel. Number of expression classes was chosen based upon least number of classes with least amount of within-class variance generated after 500 iterations.

Chl Concentration

Cells were collected by centrifugation of 1 mL of culture, and Chl was extracted in 1 mL of 80% (v/v) acetone for 20 min from pelleted samples after supernatant was removed. After extraction, samples were pelleted by centrifugation and the supernatant was used for analysis. Chl was quantified spectroscopically as described in Ritchie (2006) using a DU 800 spectrophotometer (Beckman Coulter).

Phytol Isotopic Labeling

For determination of Chl synthesis rates, ^{13}C incorporation into the phytol side chain of the Chl molecule was measured using gas chromatography (GC)/MS. Exponentially growing cells were centrifuged and transferred to $^{13}C_2$ acetate TAP medium with and without N. Two milliliters of cells (approximately 0.15 mg CDW) was harvested at various time points. Lipids were extracted with chloroform-methanol (2:1) and dried under a stream of N. The dried lipid extract was saponified using methanolic potassium hydroxide at 100°C for 2 h in a 2-mL screw-capped tube. The unsaponified components that contained the phytol chain were then extracted using hexane and dried under N. The extract was derivatized to its tetramethylsilane (TMS) derivative using 50 μL of *N*-Methyl-*N*-(trimethylsilyl)trifluoroacetamide with 1% (v/v) trimethylchlorosilane (Sigma Aldrich) by incubating at 80°C for 1 h. One microliter of the derivative was injected into the GC/MS consisting of HP 6890 GC (Hewlett Packard) equipped with a DB-5MS column (5% [w/w] phenyl-methyl-siloxan-diphenylpolysiloxan; 30 m × 0.251 mm × 0.25 μm, Agilent) and a quadrupole mass spectrometer (MS 5975, Agilent). Electron ionization was carried out at 70 eV. The separation was carried out in GC (carrier gas, 1.1 mL min^{-1} helium) with the following temperature program: initial column temperature of 100°C, increase of 20°C min^{-1} until 150°C, 4°C min^{-1} until 225°C, and 30°C min^{-1} until 325°C with a final holding time of 5 min. The inlet and quadrupole both had temperatures set to 320°C. The ions 143, 144, 145, 146, and 147 of the mass spectra were monitored, which represent a four-carbon fragment of the phytol chain. The obtained mass spectrometric data were corrected for the natural abundance of the elements to give fractional ^{13}C labeling.

Carotenoid Quantification

Folch extracts were analyzed for free carotenoid content via HPLC as described by Rodriguez-Uribe et al. (2012). Extracts were diluted in $CHCl_3$:MeOH (2:1, v/v), and a 20-μL aliquot was separated on a 4.6- × 250-mm carotenoid column (YMC America LLC). Carotenoid peaks were detected by a 996 photodiode array detector at 400 to 600 nm (Waters), and peak detection and integration were performed using the extracted 450-nm absorbance chromatogram. Peak areas were integrated for relative quantification by peak area using the Empower software (Waters). Astaxanthin, loroxanthin, and neoxanthin were identified by comparison of the UV absorbance spectra to their respective referenced UV spectra in Britton et al. (2009).

Lipid Analyses

Cells were centrifuged at 0°C, and lyophilized and total lipids were extracted from approximately 10 mg of dry cell mass by the method of Folch et al. (1957). Briefly, the lyophilized tissue was weighed into 2-mL Eppendorf vials and extracted with 200 μL of $CHCl_3$:MeOH (2:1, v/v) shaking on a vortexer for 30 min. The sample was then centrifuged, and the supernatant was collected, dried under N, and stored at –20°C until analysis. Thylakoid membrane lipids were quantified by direct infusion into a Fourier Transform-Ion Cyclotron Resonance MS as previously described (Holguin and Schaub, 2013).

Electron Microscopy

During N deprivation at selected time points, 50 mL of cells at 0.2 optical density of 750 nm was harvested, pelleted, and resuspended in fixation solution of TAP medium with 0.5% (v/v) glutaraldehyde and 10 μL of hydrogen peroxide to 10 mL for 1 h in the dark at 4°C on a rotary plate. After fixation, cells were pelleted (3,500 rpm) and then resuspended in 0.5 mL of TAP medium. Cells were packaged at Michigan State University and sent to Cambridge, United Kingdom for analysis. Fixed cell samples were then treated with 1% (v/v) osmium ferricyanide at 25°C for 2 h and rinsed in deionized water five times. Pelleted cells were then treated with 2% uranyl acetate in 0.05 M maleate buffer at pH 5.5 for 2 h at 25°C. They were again rinsed in deionized water, dehydrated in an ascending series of ethanol solutions from 70% to 100% (v/v), and then treated with two changes of dry acetonitrile and infiltration with Quetol epoxy resin. Sections were cut at 50 nm on a Leica Ultracut S. Samples were stained with uranyl acetate and lead citrate and viewed at 120 kV in an FEI Tecnai G2. Images were captured with an AMT XR60B camera using Deben software.

Oxygen Evolution and Consumption

Changes in dissolved oxygen was measured with an NEOFOX analyzer FOXY-R probe with a FOXY-AF-MG coating (Ocean Optics). Probe was placed in 2 mL of culture in a capped 3-mL cuvette with stir bar to keep samples mixed. Net oxygen evolution was measured for 5 min at 160 μE m^{-2} s^{-1}, and consumption was measured in the dark immediately after the light period for 1 min. Gross oxygen evolution was calculated as net oxygen evolution minus consumption.

In Vivo Spectroscopy

All spectroscopic measurements were performed with biological triplicates at each time point. Light-induced absorbance and Chl fluorescence yield were measured using a kinetic spectrophotometer/fluorometer (Sacksteder et al., 2001; Livingston et al., 2010; Hall C et al., 2011) modified for liquid samples by replacing the leaf holder with a temperature-controlled, stirring-enabled cuvette holder (standard 1-cm path length). Cells were treated with a far-red light light-emitting diode (LED; 730 nm) in otherwise darkness for 20 min to oxidize the plastoquinone pool for accurate minimal fluorescence measurements. After dark/far-red adaptation, the first saturating pulse for Chl fluorescence measurements was taken with a pulsed measuring beam (505-nm peak-emission LED) filtered through a BG18 (Edmund Optics) glass filter. The sample was then illuminated with 160 μmol photons m^{-2} s^{-1} of photosynthetic photon flux density, provided by a pair of LEDs (Luxeon III LXHL-PD09, Philips) with maximal emission at 620 nm, directed toward opposite sides of the cuvette, perpendicular to the measuring beam. Fluorescence yields from saturating pulses were measured under actinic light and averaged over six measurements, separated by 120-s intervals. Both absorption and fluorescence measuring pulses were 20 to 35 μs in duration and attenuated to produce less than a 0.1% increase in Chl fluorescence yield in dark-adapted samples. The first dark-interval relaxation kinetics trace measuring the ECS kinetics (one trace per biological replicate) was measured after 3 min of actinic illumination, followed by 1 min of actinic light. Actinic LEDs were calibrated using a Licor LI190 PAR quantum sensor.

The kinetics of PSI primary donor ($P700^+$) oxidation/reduction kinetics measurements were performed 5 min after the cells had been treated with 10 μM 3(3,4-dichlorophenyl)-1,1-dimethylurea (Sigma Aldrich) as described in Lucker and Kramer (2013). Briefly, absorbance changes attributed to P700 redox changes were monitored using a measuring LED (peak emission, 720 nm) filtered through a 5-nm band pass filter centered at 700 nm, giving an emission peak at approximately 705 nm. A Schott RG695 color glass filter was used to protect the detector from actinic light. The kinetics of $P700^+$ reduction were measured by the absorbance changes during light-to-dark transition after 10 s of actinic illumination with 160 μmol photons m^{-2} s^{-1}.

77-K Chl Fluorescence Emission Spectra

Cell cultures were taken directly from the incubator at the specified times and poured into a 3-mL styrene cuvette in triplicates at 3 μg Chl mL^{-1}. The cuvettes were immediately placed in a liquid N-filled Dewar, freezing the cells, and then stored at –80°C until further analysis. Immediate freezing of samples was important to prevent state transitions. For analysis, cuvettes were placed in a liquid N-filled Dewar. A beam of blue excitation light from an LED (peak, 440 nm) was directed through an optic fiber (Murakami, 1997). Fluorescence emission spectra from 187 to 1,110 nm were detected using a fiber optic spectrophotometer (USB2000+ UV-VIS, Ocean Optics; Hill et al., 2012).

To determine relative intensity values, data from a TAP medium blank was first subtracted. Samples were then normalized to the 685 nm (PSII-associated peak). PSI-associated fluorescence was maximal at 715 nm and was used from comparison between samples.

^{13}C Bicarbonate Labeling

^{13}C bicarbonate from a stock solution was added to a final concentration of 17 mM to 400-mL cultures of cells growing with or without N for 6 h. Cells were harvested at 0, 1, 2.5, 5, 7, 10, and 15 min after the addition of label by quenching 40-mL culture aliquots with 10 mL of methanol at –80°C. Samples were centrifuged at 0°C, the supernatant was discarded, intracellular metabolites were extracted with 100% methanol, and then extracts were dried under a stream of N_2. Methoxyamine-pyridine (50 μL of a 25-mg methoxyamine-HCl mL^{-1} solution in pyridine) was added to the dried extract and incubated for 45 min at 80°C, followed by TMS derivatization as described above for phytol analysis. One microliter of derivative was used for GC-MS. For gas chromatographic separation, helium was the carrier gas at a flow rate of 1.1 mL min^{-1}, with the following temperature program: initial column temperature of 100°C, increasing at 10°C min^{-1} to 325°C with a final holding time of 5 min. The inlet and quadrupole had temperatures of 320°C. Ions corresponding to TMS derivatives of amino acids and sugar phosphates were monitored and corrected for the natural abundance of the elements to give fractional ^{13}C labeling.

Starch Analysis

Total Glc contained in starch was measured after amyloglucosidase and amylase digestion with the Megazyme total starch analysis kit, similar to Work et al. (2010). Briefly, starch pellets remaining after methanol:chloroform (2:1) lipid extraction was autoclaved for 1 h in 0.1 M acetate buffer (pH 4.8) and then was treated with α-amylase and amyloglucosidase for 1 h at 55°C. Free Glc was quantitated with a colorimetric assay at 510 nm as described in the Total Starch Assay kit (Megazyme).

Supplemental Data

The following supplemental materials are available.

Supplemental Figure S1. Photosynthetic transcripts and protein expression.

Supplemental Figure S2. Carotenoid levels at successive times following N deprivation determined by extraction, HPLC separation, and measurement of absorbance at 450 nm compared with authentic standards.

Supplemental Figure S3. Relative changes in thylakoid lipid levels.

Supplemental Figure S4. Relative amount of oxidized Q_A based upon the lake model.

Supplemental Figure S5. PSII-inhibited P700/ν_{H^+} during N deprivation.

Supplemental Table S1. The levels of transcripts and proteins of photosynthetic pigment metabolism and starch metabolism.

ACKNOWLEDGMENTS

We thank Dr. Bruria Shachar-Hill for electron microscopy.

Received September 22, 2014; accepted December 1, 2014; published December 8, 2014.

LITERATURE CITED

Allen MM, Smith AJ (1969) Nitrogen chlorosis in blue-green algae. Arch Mikrobiol **69:** 114–120

Alric J (2010) Cyclic electron flow around photosystem I in unicellular green algae. Photosynth Res **106:** 47–56

Alvarez S, Hicks LM, Pandey S (2011) ABA-dependent and -independent G-protein signaling in Arabidopsis roots revealed through an iTRAQ proteomics approach. J Proteome Res **10:** 3107–3122

Atabani AE, Silitonga AS, Badruddin IA, Mahlia TMI, Masjuki HH, Mekhilef S (2012) A comprehensive review on biodiesel as an alternative energy resource and its characteristics. Renew Sustain Energy Rev **16:** 2070–2093

Avenson TJ, Cruz JA, Kanazawa A, Kramer DM (2005) Regulating the proton budget of higher plant photosynthesis. Proc Natl Acad Sci USA **102:** 9709–9713

Bailleul B, Cardol P, Breyton C, Finazzi G (2010) Electrochromism: a useful probe to study algal photosynthesis. Photosynth Res **106:** 179–189

Baker NR (2008) Chlorophyll fluorescence: a probe of photosynthesis in vivo. Annu Rev Plant Biol **59:** 89–113

Baker NR, Harbinson J, Kramer DM (2007) Determining the limitations and regulation of photosynthetic energy transduction in leaves. Plant Cell Environ **30:** 1107–1125

Beardall J, Griffiths H, Raven JA (1982) Carbon isotope discrimination and the CO_2 accumulating mechanism in *Chlorella emersonii*. J Exp Bot **33:** 729–737

Beardall J, Roberts S, Millhouse J (1991) Effects of nitrogen limitation on uptake of inorganic carbon and specific activity of ribulose-1,5-bisphosphate carboxylase oxygenase in green microalgae. Canadian Journal of Botany-Revue Canadienne De Botanique **69:** 1146–1150

Benning C (2010) The anionic chloroplast membrane lipids: phosphatidylglycerol and sulfoquinovosyldiacylglycerol. *In* CA Rebeiz, C Benning, HJ Bohnert, H Daniell, JK Hoober, HK Lichtenthaler, AR Portis, BC Tripathy, eds, Chloroplast: Basics and Applications, Vol 31. Springer, Dordrecht, The Netherlands, pp 171–183

Berges JA, Charlebois DO, Mauzerall DC, Falkowski PG (1996) Differential effects of nitrogen limitation on photosynthetic efficiency of photosystems I and II in microalgae. Plant Physiol **110:** 689–696

Blaby IK, Glaesener AG, Mettler T, Fitz-Gibbon ST, Gallaher SD, Liu B, Boyle NR, Kropat J, Stitt M, Johnson S, et al (2013) Systems-level analysis of nitrogen starvation-induced modifications of carbon metabolism in a *Chlamydomonas reinhardtii* starchless mutant. Plant Cell **25:** 4305–4323

Bölling C, Fiehn O (2005) Metabolite profiling of *Chlamydomonas reinhardtii* under nutrient deprivation. Plant Physiol **139:** 1995–2005

Bonente G, Passarini F, Cazzaniga S, Mancone C, Buia MC, Tripodi M, Bassi R, Caffarri S (2008) The occurrence of the psbS gene product in *Chlamydomonas reinhardtii* and in other photosynthetic organisms and its correlation with energy quenching. Photochem Photobiol **84:** 1359–1370

Boudière L, Michaud M, Petroutsos D, Rébeillé F, Falconet D, Bastien O, Roy S, Finazzi G, Rolland N, Jouhet J, et al (2013) Glycerolipids in photosynthesis: composition, synthesis and trafficking. Biochim Biophys Acta **1837:** 470–480

Britton G, Liaaen-Jensen S, Pfander H (2009) Carotenoids Volume 5. Nutr Health **5:** 409–422

Cardol P, Bailleul B, Rappaport F, Derelle E, Béal D, Breyton C, Bailey S, Wollman FA, Grossman A, Moreau H, et al (2008) An original adaptation of photosynthesis in the marine green alga *Ostreococcus*. Proc Natl Acad Sci USA **105:** 7881–7886

Chisti Y (2007) Biodiesel from microalgae. Biotechnol Adv **25:** 294–306

Coleman JR, Berry JA, Togasaki RK, Grossman AR (1984) Identification of extracellular carbonic anhydrase of *Chlamydomonas reinhardtii*. Plant Physiol **76:** 472–477

Collier JL, Grossman AR (1992) Chlorosis induced by nutrient deprivation in *Synechococcus* sp. strain PCC 7942: not all bleaching is the same. J Bacteriol **174:** 4718–4726

de Vitry C, Olive J, Drapier D, Recouvreur M, Wollman FA (1989) Post-translational events leading to the assembly of photosystem II protein complex: a study using photosynthesis mutants from *Chlamydomonas reinhardtii*. J Cell Biol **109:** 991–1006

Dent RM, Han M, Niyogi KK (2001) Functional genomics of plant photosynthesis in the fast lane using *Chlamydomonas reinhardtii*. Trends Plant Sci **6:** 364–371

Depège N, Bellafiore S, Rochaix JD (2003) Role of chloroplast protein kinase Stt7 in LHCII phosphorylation and state transition in *Chlamydomonas*. Science **299:** 1572–1575

Dong HP, Williams E, Wang DZ, Xie ZX, Hsia RC, Jenck A, Halden R, Li J, Chen F, Place AR (2013) Responses of *Nannochloropsis oceanica* IMET1 to long-term nitrogen starvation and recovery. Plant Physiol **162:** 1110–1126

Fan J, Yan C, Andre C, Shanklin J, Schwender J, Xu C (2012) Oil accumulation is controlled by carbon precursor supply for fatty acid synthesis in *Chlamydomonas reinhardtii*. Plant Cell Physiol **53:** 1380–1390

Feng X, Tang KH, Blankenship RE, Tang YJ (2010) Metabolic flux analysis of the mixotrophic metabolisms in the green sulfur bacterium *Chlorobaculum tepidum*. J Biol Chem **285:** 39544–39550

Fischer BB, Dayer R, Schwarzenbach Y, Lemaire SD, Behra R, Liedtke A, Eggen RI (2009) Function and regulation of the glutathione peroxidase homologous gene GPXH/GPX5 in *Chlamydomonas reinhardtii*. Plant Mol Biol **71:** 569–583

Folch J, Lees M, Sloane Stanley GH (1957) A simple method for the isolation and purification of total lipides from animal tissues. J Biol Chem **226:** 497–509

Frentzen M (2004) Phosphatidylglycerol and sulfoquinovosyldiacylglycerol: anionic membrane lipids and phosphate regulation. Curr Opin Plant Biol **7:** 270–276

Geider RJ, Macintyre HL, Graziano LM, McKay RML (1998) Responses of the photosynthetic apparatus of *Dunaliella tertiolecta* (Chlorophyceae) to nitrogen and phosphorus limitation. Eur J Phycol **33:** 315–332

Geiger DR, Servaites JC (1994) Diurnal regulation of photosynthetic carbon metabolism in C-3 plants. Annu Rev Plant Physiol Plant Mol Biol **45:** 235–256

Genty B, Briantais JM, Baker NR (1989) The relationship between the quantum yield of photosynthetic electron-transport and quenching of chlorophyll fluorescence. Biochim Biophys Acta **990:** 87–92

Gilmore AM, Yamamoto HY (1993) Linear models relating xanthophylls and lumen acidity to non-photochemical fluorescence quenching. Evidence that antheraxanthin explains zeaxanthin-independent quenching. Photosynth Res **35:** 67–78

Goodenough U, Blaby I, Casero D, Gallaher SD, Goodson C, Johnson S, Lee JH, Merchant SS, Pellegrini M, Roth R, et al (2014) The path to triacylglyceride obesity in the sta6 strain of *Chlamydomonas reinhardtii*. Eukaryot Cell **13:** 591–613

Gorman DS, Levine RP (1965) Cytochrome f and plastocyanin: their sequence in the photosynthetic electron transport chain of *Chlamydomonas reinhardi*. Proc Natl Acad Sci USA **54:** 1665–1669

Granum E, Kirkvold S, Myklestad SM (2002) Cellular and extracellular production of carbohydrates and amino acids by the marine diatom *Skeletonema costatum*: diel variations and effects of N depletion. Mar Ecol Prog Ser **242:** 83–94

Grossman A (2000) Acclimation of *Chlamydomonas reinhardtii* to its nutrient environment. Protist **151:** 201–224

Grossman AR, Gonzalez-Ballester D, Shibagaki N, Pootakham W, Moseley J, Pootakham W (2010) Responses to macronutrient deprivation. *In* A Pareek, SK Sopory, HJ Bohnert, X Govindjee, eds. Abiotic Stress Adaptation in Plants: Physiological, Molecular and Genomic Foundation. Springer, NY, pp 307–348

Hall C, Cruz J, Wood M, Zegara R, De Mars D, Carpenter J, Kanazawa ADK (2011) Photosynthesis: Research for Food, Fuel and Future. 15th International Conference on Photosynthesis. Zhejiang University Press, Beijing, pp 184–188

Harris EH, Stern DB, Witman GB, editors (2009) The Chlamydomonas Sourcebook, Vol. 2. Elsevier, Oxford, UK, pp 1–1071

He R, Kim MJ, Nelson W, Balbuena TS, Kim R, Kramer R, Crow JA, May GD, Thelen JJ, Soderlund CA, et al (2012) Next-generation sequencing-based transcriptomic and proteomic analysis of the common reed, *Phragmites australis* (Poaceae), reveals genes involved in invasiveness and rhizome specificity. Am J Bot **99:** 232–247

Hertle AP, Blunder T, Wunder T, Pesaresi P, Pribil M, Armbruster U, Leister D (2013) PGRL1 is the elusive ferredoxin-plastoquinone reductase in photosynthetic cyclic electron flow. Mol Cell **49:** 511–523

Hill R, Larkum AWD, Prasil O, Kramer DM, Szabo M, Kumar V, Ralph PJ (2012) Light-induced dissociation of antenna complexes in the symbionts of scleractinian corals correlates with sensitivity to coral bleaching. Coral Reefs **31:** 963–975

Holguin FO, Schaub T (2013) Characterization of microalgal lipid feedstock by direct-infusion FT-ICR mass spectrometry. Algal Research **2:** 43–50

Horton P, Ruban AV, Walters RG (1994) Regulation of light harvesting in green plants (indication by nonphotochemical quenching of chlorophyll fluorescence). Plant Physiol **106:** 415–420

Houille-Vernes L, Rappaport F, Wollman FA, Alric J, Johnson X (2011) Plastid terminal oxidase 2 (PTOX2) is the major oxidase involved in chlororespiration in *Chlamydomonas*. Proc Natl Acad Sci USA **108:** 20820–20825

Hu Q, Sommerfeld M, Jarvis E, Ghirardi M, Posewitz M, Seibert M, Darzins A (2008) Microalgal triacylglycerols as feedstocks for biofuel production: perspectives and advances. Plant J **54:** 621–639

Iwai M, Takahashi Y, Minagawa J (2008) Molecular remodeling of photosystem II during state transitions in *Chlamydomonas reinhardtii*. Plant Cell **20:** 2177–2189

Jahns P, Holzwarth AR (2012) The role of the xanthophyll cycle and of lutein in photoprotection of photosystem II. Biochim Biophys Acta **1817:** 182–193

Jamers A, Blust R, De Coen W (2009) Omics in algae: paving the way for a systems biological understanding of algal stress phenomena? Aquat Toxicol **92:** 114–121

Jans F, Mignolet E, Houyoux PA, Cardol P, Ghysels B, Cuiné S, Cournac L, Peltier G, Remacle C, Franck F (2008) A type II NAD(P)H dehydrogenase mediates light-independent plastoquinone reduction in the chloroplast of *Chlamydomonas*. Proc Natl Acad Sci USA **105:** 20546–20551

Jarvis P, Dörmann P, Peto CA, Lutes J, Benning C, Chory J (2000) Galactolipid deficiency and abnormal chloroplast development in the Arabidopsis MGD synthase 1 mutant. Proc Natl Acad Sci USA **97:** 8175–8179

Johnson X, Alric J (2012) Interaction between starch breakdown, acetate assimilation, and photosynthetic cyclic electron flow in *Chlamydomonas reinhardtii*. J Biol Chem **287:** 26445–26452

Johnson X, Alric J (2013) Central carbon metabolism and electron transport in *Chlamydomonas reinhardtii*: metabolic constraints for carbon partitioning between oil and starch. Eukaryot Cell **12:** 776–793

Johnson X, Steinbeck J, Dent RM, Takahashi H, Richaud P, Ozawa S, Houille-Vernes L, Petroutsos D, Rappaport F, Grossman AR, et al (2014) Proton gradient regulation 5-mediated cyclic electron flow under ATP- or redox-limited conditions: a study of *ΔATpase pgr5* and *ΔrbcL pgr5* mutants in the green alga *Chlamydomonas reinhardtii*. Plant Physiol **165:** 438–452

Jones MR (2007) Lipids in photosynthetic reaction centres: structural roles and functional holes. Prog Lipid Res **46:** 56–87

Klein U (1987) Intracellular carbon partitioning in *Chlamydomonas reinhardtii*. Plant Physiol **85:** 892–897

Kramer DM, Johnson G, Kiirats O, Edwards GE (2004) New fluorescence parameters for the determination of Q(A) redox state and excitation energy fluxes. Photosynth Res **79:** 209–218

Lee Y, Park JJ, Barupal DK, Fiehn O (2012) System response of metabolic networks in *Chlamydomonas reinhardtii* to total available ammonium. Mol Cell Proteomics **11:** 973–988

Leng J, Sakurai I, Wada H, Shen JR (2008) Effects of phospholipase and lipase treatments on photosystem II core dimer from a thermophilic cyanobacterium. Photosynth Res **98:** 469–478

Li X, Moellering ER, Liu B, Johnny C, Fedewa M, Sears BB, Kuo MH, Benning C (2012) A galactoglycerolipid lipase is required for triacylglycerol accumulation and survival following nitrogen deprivation in *Chlamydomonas reinhardtii*. Plant Cell **24:** 4670–4686

Li Y, Han D, Hu G, Sommerfeld M, Hu Q (2010) Inhibition of starch synthesis results in overproduction of lipids in *Chlamydomonas reinhardtii*. Biotechnol Bioeng **107:** 258–268

Liu B, Benning C (2013) Lipid metabolism in microalgae distinguishes itself. Curr Opin Biotechnol **24:** 300–309

Livingston AK, Cruz JA, Kohzuma K, Dhingra A, Kramer DM (2010) An *Arabidopsis* mutant with high cyclic electron flow around photosystem I (*hcef*) involving the NADPH dehydrogenase complex. Plant Cell **22:** 221–233

Lohr M (2009) Carotenoids. *In* D Stern, G Witman, EH Harris, eds, The Chlamydomonas Sourcebook, Ed 2. Academic Press, London, pp 799–817

Longworth J, Noirel J, Pandhal J, Wright PC, Vaidyanathan S (2012) HILIC- and SCX-based quantitative proteomics of *Chlamydomonas reinhardtii* during nitrogen starvation induced lipid and carbohydrate accumulation. J Proteome Res **11:** 5959–5971

Lucker B, Kramer DM (2013) Regulation of cyclic electron flow in *Chlamydomonas reinhardtii* under fluctuating carbon availability. Photosynth Res **117:** 449–459

Martin NC, Goodenough UW (1975) Gametic differentiation in *Chlamydomonas reinhardtii*. I. Production of gametes and their fine structure. J Cell Biol **67:** 587–605

Maruyama S, Tokutsu R, Minagawa J (2014) Transcriptional regulation of the stress-responsive light harvesting complex genes in *Chlamydomonas reinhardtii*. Plant Cell Physiol **55:** 1304–1310

Merchant SS, Helmann JD (2012) Elemental economy: microbial strategies for optimizing growth in the face of nutrient limitation. Adv Microb Physiol **60:** 91–210

Merchant SS, Kropat J, Liu B, Shaw J, Warakanont J (2012) TAG, you're it! *Chlamydomonas* as a reference organism for understanding algal triacylglycerol accumulation. Curr Opin Biotechnol **23:** 352–363

Merchant SS, Prochnik SE, Vallon O, Harris EH, Karpowicz SJ, Witman GB, Terry A, Salamov A, Fritz-Laylin LK, Maréchal-Drouard L, et al (2007) The *Chlamydomonas* genome reveals the evolution of key animal and plant functions. Science **318:** 245–250

Miller R, Wu G, Deshpande RR, Vieler A, Gärtner K, Li X, Moellering ER, Zäuner S, Cornish AJ, Liu B, et al (2010) Changes in transcript abundance in *Chlamydomonas reinhardtii* following nitrogen deprivation predict diversion of metabolism. Plant Physiol **154:** 1737–1752

Mizusawa N, Wada H (2012) The role of lipids in photosystem II. Biochim Biophys Acta **1817:** 194–208

Moseley JL, Allinger T, Herzog S, Hoerth P, Wehinger E, Merchant S, Hippler M (2002) Adaptation to Fe-deficiency requires remodeling of the photosynthetic apparatus. EMBO J **21:** 6709–6720

Msanne J, Xu D, Konda AR, Casas-Mollano JA, Awada T, Cahoon EB, Cerutti H (2012) Metabolic and gene expression changes triggered by nitrogen deprivation in the photoautotrophically grown microalgae *Chlamydomonas reinhardtii* and *Coccomyxa* sp. C-169. Phytochemistry **75:** 50–59

Müller P, Li XP, Niyogi KK (2001) Non-photochemical quenching. A response to excess light energy. Plant Physiol **125:** 1558–1566

Munekage Y, Hojo M, Meurer J, Endo T, Tasaka M, Shikanai T (2002) PGR5 is involved in cyclic electron flow around photosystem I and is essential for photoprotection in Arabidopsis. Cell **110:** 361–371

Murakami A (1997) Quantitative analysis of 77K fluorescence emission spectra in *Synechocystis* sp. PCC 6714 and *Chlamydomonas reinhardtii* with variable PS I/PS II stoichiometries. Photosynth Res **53:** 141–148

Myouga F, Hosoda C, Umezawa T, Iizumi H, Kuromori T, Motohashi R, Shono Y, Nagata N, Ikeuchi M, Shinozaki K (2008) A heterocomplex of iron superoxide dismutases defends chloroplast nucleoids against oxidative stress and is essential for chloroplast development in *Arabidopsis*. Plant Cell **20:** 3148–3162

Nguyen HM, Baudet M, Cuiné S, Adriano JM, Barthe D, Billon E, Bruley C, Beisson F, Peltier G, Ferro M, et al (2011) Proteomic profiling of oil bodies isolated from the unicellular green microalga *Chlamydomonas reinhardtii*: with focus on proteins involved in lipid metabolism. Proteomics **11:** 4266–4273

Niyogi KK, Bjorkman O, Grossman AR (1997) *Chlamydomonas* xanthophyll cycle mutants identified by video imaging of chlorophyll fluorescence quenching. Plant Cell **9:** 1369–1380

Ohlrogge J, Allen D, Berguson B, Dellapenna D, Shachar-Hill Y, Stymne S (2009) Energy. Driving on biomass. Science **324:** 1019–1020

Park J, Wang H, Gargouri M, Deshpande R, Skepper J, Holguin FO, Juergens M, Shachar-Hill Y, Hicks L, Gang DR (December 17, 2014) The response of *Chlamydomonas reinhardtii* to nitrogen deprivation: a systems biology analysis. Plant J http://dx.doi.org/10.1111/tpj.12747

Peers G, Truong TB, Ostendorf E, Busch A, Elrad D, Grossman AR, Hippler M, Niyogi KK (2009) An ancient light-harvesting protein is critical for the regulation of algal photosynthesis. Nature **462:** 518–521

Peltier G, Schmidt GW (1991) Chlororespiration: an adaptation to nitrogen deficiency in *Chlamydomonas reinhardtii*. Proc Natl Acad Sci USA **88:** 4791–4795

Petroutsos D, Terauchi AM, Busch A, Hirschmann I, Merchant SS, Finazzi G, Hippler M (2009) PGRL1 participates in iron-induced remodeling of the photosynthetic apparatus and in energy metabolism in *Chlamydomonas reinhardtii*. J Biol Chem **284:** 32770–32781

Pfalz J, Liebers M, Hirth M, Grübler B, Holtzegel U, Schröter Y, Dietzel L, Pfannschmidt T (2012) Environmental control of plant nuclear gene expression by chloroplast redox signals. Front Plant Sci **3:** 257

Philipps G, Happe T, Hemschemeier A (2012) Nitrogen deprivation results in photosynthetic hydrogen production in *Chlamydomonas reinhardtii*. Planta **235:** 729–745

Plumley FG, Douglas SE, Switzer AB, Schmidt GW (1989) Nitrogen-dependent biogenesis of chlorophyll-protein complexes. Plant Biology (New York) **8:** 311–329

Plumley FG, Schmidt GW (1989) Nitrogen-dependent regulation of photosynthetic gene expression. Proc Natl Acad Sci USA **86:** 2678–2682

Ritchie RJ (2006) Consistent sets of spectrophotometric chlorophyll equations for acetone, methanol and ethanol solvents. Photosynth Res **89:** 27–41

Rochaix JD (2002) *Chlamydomonas*, a model system for studying the assembly and dynamics of photosynthetic complexes. FEBS Lett **529:** 34–38

Rodriguez-Uribe L, Guzman I, Rajapakse W, Richins RD, O'Connell MA (2012) Carotenoid accumulation in orange-pigmented *Capsicum annuum* fruit, regulated at multiple levels. J Exp Bot **63:** 517–526

Roessler PG (1990) Environmental control of glycerolipid metabolism in microalgae: commercial implications and future research directions. J Phycol **26:** 393–399

Rumeau D, Peltier G, Cournac L (2007) Chlororespiration and cyclic electron flow around PSI during photosynthesis and plant stress response. Plant Cell Environ **30:** 1041–1051

Sacksteder CA, Jacoby ME, Kramer DM (2001) A portable, non-focusing optics spectrophotometer (NoFOSpec) for measurements of steady-state absorbance changes in intact plants. Photosynth Res **70:** 231–240

Schmollinger S, Mühlhaus T, Boyle NR, Blaby IK, Casero D, Mettler T, Moseley JL, Kropat J, Sommer F, Strenkert D, et al (2014) Nitrogen-sparing mechanisms in *Chlamydomonas* affect the transcriptome, the proteome, and photosynthetic metabolism. Plant Cell **26:** 1410–1435

Shastri AA, Morgan JA (2007) A transient isotopic labeling methodology for ^{13}C metabolic flux analysis of photoautotrophic microorganisms. Phytochemistry **68:** 2302–2312

Shifrin NS, Chisholm SW (1981) Phytoplankton lipids: interspecific differences and effects of nitrate, silicate and light-dark cycles. J Phycol **17:** 374–384

Shimojima M, Ohta H, Nakamura Y (2010) Biosynthesis and Function of Chloroplast Lipids. *In* H Wada, N Murata, eds, Lipids in Photosynthesis, Vol 30. Springer, Dordrecht, The Netherlands, pp 35–55

Siaut M, Cuiné S, Cagnon C, Fessler B, Nguyen M, Carrier P, Beyly A, Beisson F, Triantaphylidès C, Li-Beisson Y, et al (2011) Oil accumulation in the model green alga *Chlamydomonas reinhardtii*: characterization, variability between common laboratory strains and relationship with starch reserves. BMC Biotechnol **11:** 7

Simionato D, Block MA, La Rocca N, Jouhet J, Maréchal E, Finazzi G, Morosinotto T (2013) The response of *Nannochloropsis gaditana* to nitrogen starvation includes de novo biosynthesis of triacylglycerols, a decrease of chloroplast galactolipids, and reorganization of the photosynthetic apparatus. Eukaryot Cell **12:** 665–676

Takaichi S (2011) Carotenoids in algae: distributions, biosyntheses and functions. Mar Drugs **9:** 1101–1118

Tokutsu R, Minagawa J (2013) Energy-dissipative supercomplex of photosystem II associated with LHCSR3 in *Chlamydomonas reinhardtii*. Proc Natl Acad Sci USA **110:** 10016–10021

Tunçay H, Findinier J, Duchêne T, Cogez V, Cousin C, Peltier G, Ball SG, Dauvillée D (2013) A forward genetic approach in *Chlamydomonas reinhardtii* as a strategy for exploring starch catabolism. PLoS ONE **8:** e74763

Turkina MV, Kargul J, Blanco-Rivero A, Villarejo A, Barber J, Vener AV (2006) Environmentally modulated phosphoproteome of photosynthetic membranes in the green alga *Chlamydomonas reinhardtii*. Mol Cell Proteomics **5:** 1412–1425

Urzica EI, Vieler A, Hong-Hermesdorf A, Page MD, Casero D, Gallaher SD, Kropat J, Pellegrini M, Benning C, Merchant SS (2013) Remodeling of membrane lipids in iron-starved *Chlamydomonas*. J Biol Chem **288:** 30246–30258

Van K, Spalding MH (1999) Periplasmic carbonic anhydrase structural gene (*Cah1*) mutant in *Chlamydomonas reinhardtii*. Plant Physiol **120:** 757–764

Wang H, Alvarez S, Hicks LM (2012) Comprehensive comparison of iTRAQ and label-free LC-based quantitative proteomics approaches using two *Chlamydomonas reinhardtii* strains of interest for biofuels engineering. J Proteome Res **11:** 487–501

Wang Y, Duanmu D, Spalding MH (2011) Carbon dioxide concentrating mechanism in *Chlamydomonas reinhardtii*: inorganic carbon transport and CO_2 recapture. Photosynth Res **109:** 115–122

Wang ZT, Ullrich N, Joo S, Waffenschmidt S, Goodenough U (2009) Algal lipid bodies: stress induction, purification, and biochemical characterization in wild-type and starchless *Chlamydomonas reinhardtii*. Eukaryot Cell **8:** 1856–1868

Wijffels RH, Barbosa MJ (2010) An outlook on microalgal biofuels. Science **329:** 796–799

Williams PJL, Laurens LML (2010) Microalgae as biodiesel and biomass feedstocks: review and analysis of the biochemistry, energetics and economics. Energy & Environmental Science **3:** 554–590

Work VH, Radakovits R, Jinkerson RE, Meuser JE, Elliott LG, Vinyard DJ, Laurens LM, Dismukes GC, Posewitz MC (2010) Increased lipid accumulation in the *Chlamydomonas reinhardtii* sta7-10 starchless isoamylase mutant and increased carbohydrate synthesis in complemented strains. Eukaryot Cell **9:** 1251–1261

Wykoff DD, Davies JP, Melis A, Grossman AR (1998) The regulation of photosynthetic electron transport during nutrient deprivation in *Chlamydomonas reinhardtii*. Plant Physiol **117:** 129–139

Yang ZK, Ma YH, Zheng JW, Yang WD, Liu JS, Li HY (2014) Proteomics to reveal metabolic network shifts towards lipid accumulation following nitrogen deprivation in the diatom *Phaeodactylum tricornutum*. J Appl Phycol **26:** 73–82

Yang ZK, Niu YF, Ma YH, Xue J, Zhang MH, Yang WD, Liu JS, Lu SH, Guan Y, Li HY (2013) Molecular and cellular mechanisms of neutral lipid accumulation in diatom following nitrogen deprivation. Biotechnol Biofuels **6:** 67

Yoshida K, Igarashi E, Mukai M, Hirata K, Miyamoto K (2003) Induction of tolerance to oxidative stress in the green alga, *Chlamydomonas reinhardtii*, by abscisic acid. Plant Cell Environ **26:** 451–457

Young EB, Beardall J (2005) Modulation of photosynthesis and inorganic carbon acquisition in a marine microalga by nitrogen, iron, and light availability. Canadian Journal of Botany-Revue Canadienne De Botanique **83:** 917–928

Young JD, Shastri AA, Stephanopoulos G, Morgan JA (2011) Mapping photoautotrophic metabolism with isotopically nonstationary ^{13}C flux analysis. Metab Eng **13:** 656–665